

Mimicking a Pathologist: Dual Attention Model for Scoring of Gigapixel Histology Images

Manahil Raza¹, Ruqayya Awan¹, R. M. Saad Bashir¹, Talha Qaiser¹ and Nasir Rajpoot¹

¹ {manahil.raza, r.awan.1, saad.bashir, talha.qaiser, n.m.rajpoot}@warwick.ac.uk

Abstract—Some major challenges associated with the automated processing of whole slide images (WSIs) includes their sheer size, different magnification levels and high resolution. Utilizing these images directly in AI frameworks is computationally expensive due to memory constraints, while downsampling WSIs incurs information loss and splitting WSIs into tiles and patches results in loss of important contextual information. We propose a novel dual attention approach, consisting of two main components, to mimic visual examination by a pathologist. The first component is a soft attention model which takes as input a high-level view of the WSI to determine various regions of interest. We employ a custom sampling method to extract diverse and spatially distinct image tiles from selected high attention areas. The second component is a hard attention classification model, which further extracts a sequence of multi-resolution glimpses from each tile for classification. Since hard attention is non-differentiable, we train this component using reinforcement learning and predict the location of glimpses without processing all patches of a given tile, thereby aligning with pathologist’s way of diagnosis. We train our components both separately and in an end-to-end fashion using a joint loss function to demonstrate the efficacy of our proposed model. We employ our proposed model on two different IHC use cases: HER2 prediction on breast cancer and prediction of Intact/Loss status of two MMR biomarkers, for colorectal cancer. We show that the proposed model achieves accuracy comparable to state-of-the-art methods while only processing a small fraction of the WSI at highest magnification.

Index Terms—Computational pathology, Dual attention, Reinforcement learning, Automated slide scoring

I. INTRODUCTION

Immunohistochemistry (IHC) refers to a way of “talking with cells” [1] and is a variant of immunostaining that has emerged as a *gold standard* in clinical cancer diagnostics. In histopathology, IHC is widely used to detect and quantify the presence of a specific protein marker for detailed disease profiling. It allows detailed assessment of the expression of various biomarkers by utilizing stains produced as a consequence of antigen and antibody reactions in the histologically relevant regions of the examined tissue sections [2]. Assessment of these biomarkers is crucial for assessing the risk, diagnosis, prognosis, response to therapy and progression of different cancers in patient management [3].

The human epidermal growth factor receptor 2 (HER2) gene has emerged as a key cell membrane biomarker and its expression is overamplified in approximately 20% of all invasive breast carcinoma (BC) cases [4]. Higher recurrence and poor survival rates have been linked with the overexpression of HER2 protein which is responsible for accelerating the growth of malignant epithelial cells [5]. However, the development of anti-HER2 treatments has significantly improved prognosis for HER2 positive patients. As such, current clinical guidelines recommend that all patients with breast cancer undergo HER2 testing which can be performed using IHC staining. Current diagnostic procedures involve the manual examination of IHC-stained HER2 slides by pathologists who assign a score (0-3+) to each slide. Fig. 1 contains examples of regions of interest (ROIs) from slides with different HER2 scores.

Similarly, the Mismatch repair (MMR) status of tumors has emerged as another promising predictive biomarker for colorectal cancer, crucial for the selection of patients for immunotherapy. MutL homologue 1 (MLH1), postmeiotic segregation increased 2 (PMS2), mutS homologue 2 (MSH2) and mutS homologue 6 (MSH6) collectively form a panel of MMR proteins responsible for rectifying any errors made during the duplication of microsatellites, repetitive nucleotide sequences in the genome. Patients with microsatellite instability (MSI) or deficient DNA mismatch repair (dMMR) have discrepancies in the length of these repeat DNA sequences and have been shown to respond favorably to immunotherapy [6]. Routinely, MMR status is assessed by performing IHC staining for all four proteins. The expression in MMR biomarkers is quantified as either positive/intact if the DAB stain detected in the cancerous nuclei is of similar or stronger intensity as in the normal tissue cells or negative/loss if weak staining is detected in the tumor nuclei in comparison to normal tissue cells. Fig. 1 shows ROIs from slides with differing MMR marker status.

Currently, a pathologist manually examines IHC stained tissue slides under a microscope in search of desired patterns and abnormalities. This is a tedious and time-consuming process and subject to inter- and intra-observer variability [7]. The advent of whole-slide image (WSI) scanners has enabled tissue glass slides to be scanned into digitized images, which initiated the adoption of Digital Pathology in routine clinical practice. The integration of WSIs into the mainstream pathology workflow has sprung forth a new and fast-expanding field of research, Computational Pathology (CPATH), which enables the quantitative assessment of slides, thus avoiding human bias and allowing precise and reproducible extraction of data from slides [8]. Recent years have seen an increased interest in

Manahil Raza, Ruqayya Awan, Raja Muhammad Saad Bashir, Talha Qaiser, and Nasir Rajpoot are from the Tissue Image Analytics Centre, Department of Computer Science, University of Warwick, UK

Nasir Rajpoot is also affiliated with The Alan Turing Institute, London, UK and also with the Department of Pathology, University Hospitals Coventry & Warwickshire, UK

applying deep learning (DL) techniques for CPATH problems. However, computational and memory requirements for direct processing of multi-gigapixel WSIs at a high magnification exceed the capabilities of current hardware devices. One of the most common approaches for the automated analysis of histopathology WSIs is to exhaustively analyze patches extracted from the entire tissue or tumor area using the “sliding window” paradigm. This method has two disadvantages: first, not all patches are diagnostically relevant and second, patches extracted from the same spatial area can potentially provide redundant information to the model. Consequently, various patch-selection strategies and attention-based methods have been proposed to alleviate the above-mentioned problems. In order to decide upon which strategy to employ, we first need to understand a pathologist’s diagnostic process.

In 1967, King *et al.* [9] raised the following question, “How does a pathologist make a diagnosis?”. This question was first answered by Pena *et al.* [10] who attempted to describe the processes by which a pathologist may reach a decision. Rather than using an exhaustive strategy wherein all possible data is examined and evaluated, analogous to the sliding window paradigm in computational pathology, an experienced pathologist may employ some “shortcuts”. Initially, pathologists may use cognitive processes such as saccades to gather information from the given histopathology slide. One of the diagnostic strategies they proposed thereafter was multiple branching wherein a conclusion is reached by investigating one of the potential paths for diagnosis, decided upon by preceding diagnostic inquiries. Another diagnostic strategy, pattern recognition, is used to identify histological patterns that match previously learned disease descriptions, a concept applied in supervised learning algorithms.

The potential integration of AI-based models in routine clinical diagnostics depends, at least in part, on the model’s ability to mimic the diagnostic procedures employed by pathologists on the WSIs. We propose a dual attention model that uses two attention mechanisms to alleviate the problems that arise from the disjoint patching dilemma, which leads to loss in visual context, important information needed to understand the spatial organization of tissue components in the tumor microenvironment (TME). The proposed workflow aims to model the aforementioned processes employed by the pathologist in routine clinical practice by sequentially predicting and analyzing some of the diagnostically relevant regions using dual visual attention and reinforcement learning. We begin by employing a soft attention module at a high level (low magnification) view of the WSI to identify potential ROIs in need of further inspection. This is analogous to a pathologist initially performing visual examination on the entire tissue slide at a low magnification and deciding upon areas in the slide which require further attention. Similar to a pathologist “zooming in” on some of the diagnostically relevant regions, we extract high-power fields (HPFs) from the most attentive areas identified by our soft attention module and pass them to the hard attention module. This module extracts a sequence of glimpses or patches at a higher magnification from the HPF in an attempt to model a sequence of saccades during visual examination. The location of each patch is decided upon by the

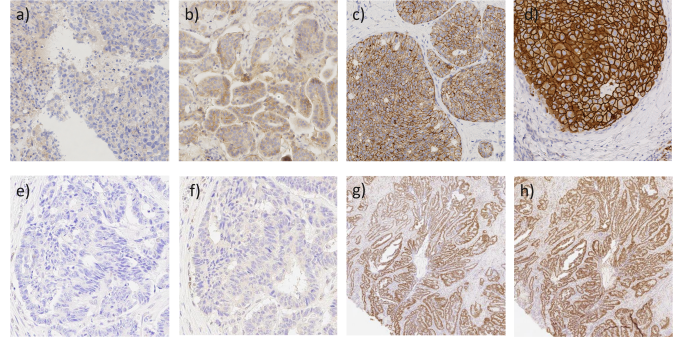


Fig. 1. Examples of regions of interest from (first row) breast cancer whole-slide images: a) HER2 Score 0, b) HER2 Score 1+, c) HER2 Score 2+, d) HER2 Score 3+ and (second row) colorectal cancer whole-slide images: e) Loss status of MLH1, f) Loss status of PMS2, g) Intact status of MLH1, h) Intact status of PMS2.

preceding glimpses, like the multiple branching technique, and information from all the glimpses is collectively processed to come to a classification decision for the HPF in question. The process is repeated iteratively until all the HPFs are processed in order to assign a slide-level score to the WSI.

Our main contributions are as follows:

- We introduce a novel dual attention model for the automated scoring of gigapixel IHC stained images using soft and hard attention to extract most informative regions of interest from the WSIs.
- We propose a dynamic joint loss function to train the model in an end-to-end fashion and enable both attention modules to be trained simultaneously.
- We validate our method on two separate IHC scoring problems, namely the prediction of HER2 Scores for breast cancer and the prediction of the Intact or Loss status for two MMR-markers in colorectal cancer.
- We demonstrate that in both use cases, the proposed method achieves performance comparable to conventional methods while only analyzing a fraction of the WSI at the highest resolution. Our proposed method for HER2 outperforms 10+ existing methods by analyzing only 5% of the WSI regions at the highest magnification.

II. RELATED WORK

Existing methods for automated processing of IHC stained histopathology WSIs can be broadly categorized into three groups: a) patch selective and patch exhaustive methods b) reinforcement learning and hard attention, and c) automated IHC scoring.

A. Patch Selective and Patch Exhaustive Methods

A straightforward approach commonly employed by several existing methods uses the classical “sliding window” paradigm to exhaustively extract patches from the tissue or tumor area. In the absence of patch-level annotations, the underlying assumption is that the image level label can be assigned to each image patch [11] [12]. However, this assumption turns a blind eye to the fact that not every patch extracted from the

tissue, or even the tumor region contributes equally to the task at hand. For example, a patch containing adipose tissue has little information about tumor grades.

Recent years have seen an increased level of interest in the application of attention mechanisms to identify important tissue regions. Soft attention networks aim to learn the weighted importance of pixels in an image. Yang *et al.* [13] used coarse region-level annotations to guide the model to focus on diagnostically relevant areas while suppressing noise for the purpose of breast cancer classification. A deep selective approach was used by Xu *et al.* [14] which made use of two networks, a soft attention classification network and a decision network which was used to “decide” if a patch could potentially improve the discriminative ability of its sister network. Kong *et al.* [15] proposed a model that successively uses attention maps to gradually “zoom in” to informative regions within the slide.

Katharopoulos *et al.* [16] proposed a novel attention sampling strategy whereby the authors used a down-sampled low resolution version of the original image to compute an attention distribution. The attention map corresponds to a probability distribution which was used to identify potential ROI. Instead of extracting all patches at high resolution the authors only extracted patches at high resolution from the original image at locations provided by the attention map. The extracted patches were used to predict the classification label of interest. Their proposed model predicted the presence of epithelial cells in H&E slides of colon cancer without having access to patch level annotations. In a similar vein, Zhang *et al.* [17] introduced a novel attention sampling method that uses a thumbnail of the original image to generate attention distributions at different magnifications. Based on the attention maps they sample patches from both different spatial locations as well as different magnifications. However, this approach involves creating multiple attention maps at different magnifications and is more computationally expensive, whereas the proposed approach only utilizes a single attention map.

B. Reinforcement Learning and Hard Attention

The application of deep reinforcement learning (DRL) techniques in the fields of medical imaging and computational pathology is a subject of considerable ongoing research. Many papers have entertained the notion of performing classification tasks, without having access to the entire image. Minh *et al.* [18] was among the seminal papers that modeled human visual perception by employing reinforcement learning concepts (REINFORCE) with a hard attention retina-inspired model on small handwritten digit images of 28×28 , by the name of recurrent attention model (RAM). Ba *et al.* [19] extended this work by proposing a deep recurrent attention model (DRAM) capable of recognizing multiple objects. Their proposed model incorporated contextual information and outperformed state-of-the-art CNNs on a house-number recognition dataset containing small images of size 54×54 .

BenTaieb *et al.* [20] extended upon the RAM and applied it to computational pathology data with the aim of predicting the presence of cancer in lymph nodes. However, they too

resorted to manual patch extraction. Xu *et al.* [21] proposed a hybrid attention model wherein a soft attention mechanism was applied to the “glimpses” or patches extracted from an image using hard attention. Their model not only selected diagnostically relevant patches but also determined discriminative regions from within those patches thereby managing to classify images while only using 15% of the images. Our approach employs soft attention rather than hard attention as the initial step. This not only allows for more interpretability regarding the relative importance of different areas in the WSI with regards to the classification task, it also allows us to sort and cluster tiles based on their attention values, to create masks for instance.

C. IHC Scoring

Mukundan *et al.* [22] proposed a set of image features inspired by the visual markers used to assess slides recommended for HER2 testing. These features included characteristic curves and rotation-invariant uniform local binary pattern curves. Rodner *et al.* [23] sampled tiles centered around a point of interest determined by a single click “probe” in the data. The respective patches were used to calculate deep bilinear features, using CNNs. Saha *et al.* [24] proposed a deep network for HER2 classification by way of cell membrane and nuclei segmentation using Trapezoidal LSTM networks. Pitkaaho *et al.* [25] used a variant of the AlexNet architecture and achieved comparable results. However, they manually selected ROI from HER2 images at a lower resolution.

The proposed model extends the work of Qaiser *et al.*, [12], which modelled the prediction of IHC scoring as a sequential learning problem. Conventionally, the histopathologist does not visually analyze each and every visual field to score the IHC slide, rather they focus on a small number of visual fields or ROIs. The model employed DRL to effectively identify ROIs by way of a parametrized policy that prevented the model from revisiting locations it had already analyzed. However, the selection of these ROI takes place in the context of a single image tile. This again necessitated the identification of tissue regions and consequently the manual and exhaustive extraction of image tiles from the identified tissue components using the sliding window paradigm. The proposed model aims to automate the tiling process and presents a cohesive end-to-end alternative thereby overcoming the challenges inherent in patch-based models.

III. METHODOLOGY : THE DUAL ATTENTION METHOD

The proposed model consists of two main components which can function simultaneously to mimic a histopathologist examining a tissue slide under the microscope. In routine clinical practice, for a given tissue slide, a pathologist usually visualizes different tissue components at a lower magnification to localize diagnostically relevant HPFs and then observes the morphological differences in selected HPFs at a higher magnification. In our proposed model, the first component is a soft attention model which takes as input a high-level (low magnification) view of the entire WSI to determine various ROIs. Image tiles (at higher magnification) are extracted from

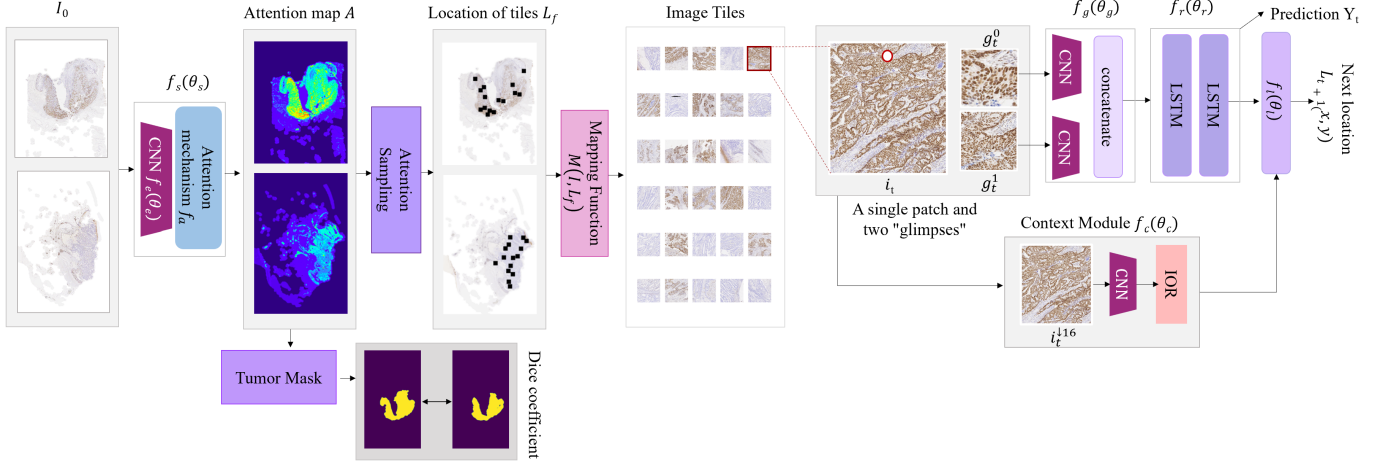


Fig. 2. An overall concept of the proposed dual attention method depicting the downsampled WSIs passed as input to the soft attention module and the resulting attention maps. The sampling method extracts image tiles from the locations depicted in the diagram using a mapping function. Each extracted image tile is passed to the hard attention module which extracts multi resolution glimpses at $20\times$ and $40\times$.

the previously selected high-attention areas for classification purposes using a custom sampling method. The second component is the classification model, which uses these image tiles and further extracts a sequence of multi-resolution glimpses or patches from these tiles. The illustration of our proposed workflow is shown in Fig. 2. In the following sections we explain both the soft and hard attention modules and their respective loss functions as well as the attention sampling procedure and the joint loss function.

A. Soft Attention Model

Inspired by [16], the Soft Attention Model (SAM) $f_s(\theta_s)$ with learnable parameters θ_s , aims to discover potential ROIs in the input image that could prove conducive to the classification task at hand. Let the WSI be denoted as $I \in R^{H \times W \times C}$ where H, W and C represent the height, width and channels of the image respectively. Due to computational and memory constraints it is not feasible to train the model with the entire WSI, at the highest magnification. To reduce the computational complexity of the proposed framework we take as input a down sampled version of the WSI scaled by a factor s , $I_0 \in R^{h \times w \times C}$ where $h \ll H$ and $w \ll W$. Let $f_e(\cdot)$ parameterized by θ_e , represent a function of feature extractor network consisting of a convolutional neural network (CNN) with ReLU non-linearities that extracts discriminative features from the input image I_0 . Employing an attention mechanism $f_a(\cdot)$ on the extracted features is similar to learning a probability distribution over the pixels of the image such that the probability always sums up to 1 as shown in (1),

$$\sum_{j=0}^N f_a(I_0, \theta_a)_j = 1 \quad (1)$$

where I_0 denotes a downsampled image passed to the model and $N = h \times w$ denotes the number of pixels. The probabilities correspond to the relevance of the areas for the classification

task. The overall definition of the proposed soft attention model is given in (2). This results in an attention map $A \in R^{h \times w}$ which highlights potentially informative regions in the image I_0 .

$$f_s(I_0, \theta_s) = f_a(f_e(I_0, \theta_e), \theta_a) \quad (2)$$

B. Attention Sampling

The attention map A contains both high and low attention regions, where the attention probabilities indicate the relative importance of different regions within the image for the classification task. Fig. 3 shows attention maps for a single slide as training progresses. We sample a set of locations from the high attention regions without replacement in order to extract a set of representative image tiles from the WSI. A major challenge in this regard is that the attention map may contain false positives for high attention regions e.g. tissues artifacts that are misclassified as ROIs due to the use of entropy. We attempt to solve this problem by adding noise to the attention distribution. In contrast to the Gumbel-max method used in [16], our custom sampling method only introduces noise within the tissue regions thereby ensuring no image tiles containing background information are used for downstream analysis.

We created a noise vector, $\mathbf{n} \in R^{h \times w}$, by generating random numbers sampled from a uniform distribution in the range $[low, high]$ where both low and $high \in R$ and $high > low$. The benefits of this scheme are two-fold, first it minimizes the effects of the false positive regions on downstream tasks and secondly it introduces diversity in the choice of informative tiles provided to the classifier during the training process. To extract the image tiles, we first normalize the attention distribution A to the range $(0, 1]$, denoted as \hat{A} using minmax normalization.

Employing our custom sampling method on two different use-cases necessitated the use of varied sampling methods.

This is due to the fact that while tumor areas generally exist in the form of a "cluster", HER2 positive score depends on the intensity of DAB staining whereas the loss/intact status of the MMR bio-markers is determined simply by the detecting the presence of DAB staining. We employed our proposed framework using two different attention refining methods.

1) *Tumor Attention Maps*: The tumor attention maps aim to identify tumor areas within the Comet-MMR slides with a reasonable degree of accuracy by detecting the presence of DAB stains. In this regard we used the k -means clustering with heuristic of putting attention map into three categories i.e. background, normal tissue and tumor areas.

2) *Positive Attention Maps*: The positive attention maps were used to locate regions within the image with the highest probability of being HER2+ by using the intensity of DAB staining. We generated a mask m by using adaptive thresholding on the normalized attention map \bar{A} to extract highly probable image tiles.

In order to focus the "noise" only on the relevant areas within the slide we multiplied the noise vector with the mask m . Additionally, we also multiplied the normalized attention map with the mask which gives us our final attention distribution $F_a = (m \times n) + (m \times \bar{A})$. Thereafter we performed top k -sampling on our final attention maps with target noise. This gives us a set of location indices. Let N be the desired number of tiles to extract from the WSI then for each image I_0 we initially sampled $2 \times N$ locations $L \in R^{N \times 2}$ from the high probability regions. Out of these $2 \times N$ locations some may be spatially close to each other thereby contributing to data redundancy. To ensure that we obtain spatially distinct tiles we initially created an empty set to represent our "shortlisted" final locations, $L_F \in R^N$. At each time-step, a location index $L_t(x, y)$ is only added to L_F if the Euclidian distance, d between the coordinates L_t and all coordinate pairs previously in L_F is greater than a certain threshold, d_t .

We define a mapping function $M(I, L_F)$ that maps each coordinate pair in $L_F = (x, y)$ to a location in the WSI $I \in R^{H \times W \times C}(X, Y)$ using a pre-defined scaling factor s between the WSI $I \in R^{H \times W \times C}$ and image $I_0 \in R^{h \times w \times C}$ [26].

The sampled image tiles of size 2048×2048 were resized to 128×128 and passed on to a second feature extractor network f_f to obtain the feature vectors. Similar to [16] the gradient of the attention distribution was derived by calculating the expectation of the sampled tiles based on their attention values.

C. Soft Attention Regularization

The soft attention mechanism represents a multinomial distribution over the pixels in the image. Let E be the multinomial entropy function for the attention maps. To ensure the attention distribution does not focus on a small number locations where it receives maximum reward, we used an entropy regularizer [16] [17]. This attempts to resolve the exploration-exploitation problem preventing the model from quickly assigning high probabilities to a few selected locations. Instead, it encourages the model to 'explore' various locations:

$$L_{SA} = \beta E(f_s(I_0; \theta_s)) \quad (3)$$

where β denotes the entropy regularizer and f_s denotes the soft attention mechanism. The above formulation results in a relatively uniform attention distribution due to the usage of entropy.

D. Hard Attention RL Model

The tiles extracted from high attention regions are still large enough to contain irrelevant areas. Moreover training a CNN directly with the tiles is still not feasible due to computational and memory constraints. Therefore, we proposed a hierarchical dual attention method that incorporates soft attention at the WSI level to extract relevant tiles and then hard attention at the tile level for the underlying task. Our soft attention module provides us with a set of N image tiles of size 2048×2048 at resolution $40x$ extracted from the WSI where we used a retina-inspired hard attention mechanism [18] in our classification model to selectively analyze informative parts of a single image tile.

The classifier used is inspired from [12]. Our model can be formalized by what is known as a Partially Observable Markov Decision Process (POMDP) in reinforcement learning literature. The image tile can be thought of as an environment and the neural networks collectively act as an agent, a decision-making entity that linearly interacts with the environment.

Considering a single image tile i sampled from I , we extract multi-resolution patches from within the tile to reach a classification decision. At each time-step t , the model receives a state from the environment, consisting of two multi-resolution glimpses centered around an individual location $l_t = (x_t, y_t)$. The two glimpses $g_t = (g_{0t}, g_{1t}) \in R^{h_g \times w_g \times C}$ of size 128×128 are extracted at resolutions $40x$ and $20x$ respectively, mimicking the peripheral vision around a single point of focus. A CNN f_g parameterized by θ_g acts as a non-linear function which takes as input these two RGB images and aggregates the features extracted from these two glimpses to create a feature representation vector v_{gt} . To capture both the semantic and spatial information, the features of the location coordinates v_{lt} are also extracted by way of a linear layer and combined with the feature vector v_{gt} to obtain $v_t = v_{gt} \times v_{lt}$. In line with our objective to mimic a pathologist's visual attention we use multiple such glimpses analogous to a sequence of saccades. An example of this sequence of glimpses can be found in Fig. 4.

The backbone of the hard attention classification model is a recurrent neural network (RNN). In the absence of unrestricted access to the entire image tile, i the RNN sequentially builds up an internal representation of the environment using glimpses. To retain information from earlier time-steps and to learn the spatial dependencies between the glimpses, we use a long short-term memory (LSTM) based RNN. At each timestep t the RNN $f_r(\theta_r)$ with learnable parameters θ_r processes the aggregated features of the glimpses to update the parameters of its internal hidden states (memory units), h_t .

$$h_{t+1} = f_r(h_t, v_t; \theta_r). \quad (4)$$

The CNN and RNN collectively act as an agent. Given the current state or "glimpse" of the environment, the agent

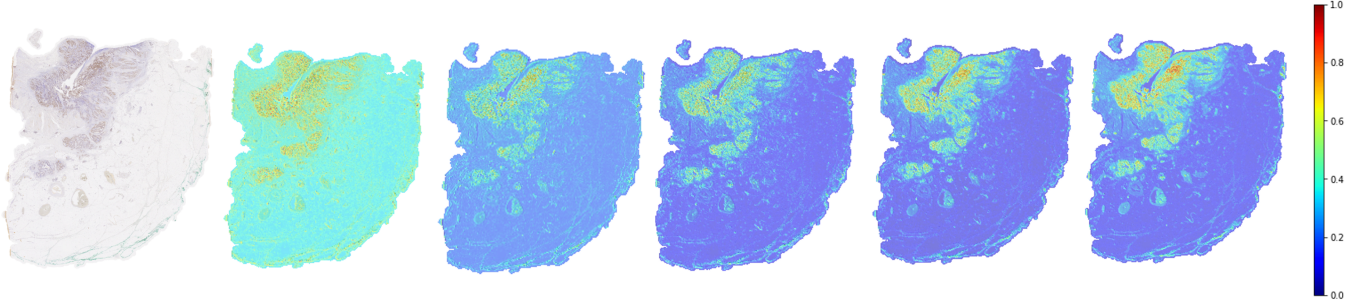


Fig. 3. (left to right) The first column shows the original MLH1 WSI. The remaining columns show the evolution of the attention maps along different epochs as training progresses for the given slide.

predicts the location of the next glimpse $l_{t+1} = (x, y)$ and a classification decision. Another CNN f_c was employed to embed contextual awareness in the model and to aid in the selection of the ROIs. This model with learnable parameters θ_c takes as input a down-scaled version of the original image tile, i_d to provide contextual information and assist in the selection of locations for the glimpses.

To ensure that the model selects spatially distinct locations an “Inhibition of Return” (IOR), which suppresses the textural information of previously visited locations by blacking out those regions, was incorporated into the process. The outputs of the last hidden layer of the recurrent neural network and the context module are combined using the Hadamard product formula to obtain a feature vector. The location network $f_l(\theta_l)$ linearly transforms the resulting feature vector to predict the next location $l_{t+1} = (x_{t+1}, y_{t+1})$.

In order to model human visual attention, the entire process is repeated iteratively for T time-steps on a single image tile. At the end of this sequence of saccades $(g_{t-1}, g_t, g_{t+1} \dots g_T)$, referred to as an “episode” in RL literature, the models predict the final classification label Y_T for the image tile i_t under consideration.

E. Hard Attention Loss function

All the individual components of the retina-inspired hard attention model were trained in an end-to-end fashion where we optimized the loss obtained from each neural network present in the overall framework i.e. the glimpse network f_g , the recurrent model f_r , the contextual CNN f_c and the location network f_l . Similar to [12] in order to optimize the loss, the hard attention model learns a parameterized DRL policy π where each state is mapped to a set of actions by maximizing the sum of the expected reward of said actions while following the parameterized policy. In our research study, the actions consist of coordinates of the next location $l_{t+1}(x_{t+1}, y_{t+1})$ from where the multi-resolution glimpses will be extracted and classification decision Y_T , provided the input is the glimpse $g_t = (g_{0t}, g_{1t})$ at time-step t from location $l_t(x_t, y_t)$ and the down sampled version of the image tile i_d .

$$\pi((l_{t+1}(x_{t+1}, y_{t+1}), Y_T)|(v_t, i_d); \theta_{HA}). \quad (5)$$

where $\theta_{HA} = \theta_g, \theta_r, \theta_c, \theta_l$. The reward is calculated using the following equation on all glimpses for a given tile.

$$r_t = \begin{cases} 1 & \text{if } GT = Y_t \\ 0 & \text{otherwise} \end{cases} \quad (6)$$

where r_t and Y_t denote the reward and predicted score for each glimpse respectively and GT denotes the ground truth.

The final reward $R_T = \sum_{t=0}^T 1_{t-1} r_t$ is calculated by taking sum of all rewards of the entire glimpse episode $(g_{t-1}, g_t, g_{t+1} \dots g_T)$, where 1 is a weighing factor (a concept commonly used in RL literature).

The parameterized policy π is optimized with the help of maximizing the model’s performance with respect to the reward and this objective can be achieved by the reverse of gradient descent. Rather, to maximize the policy gradients the REINFORCE rule has been employed where in each episodic scenario the actions leading to higher rewards are computed using the gradients and log probabilities such that the actions with low rewards are minimized. In order to reduce the intra-class variance, a common drawback of the REINFORCE method, a baseline function was introduced by normalizing the model parameters.

$$\nabla L_\theta = \sum_{t=0}^T \nabla_\theta \log \pi((l_{t+1}, Y_T)|(v_t, i_d); \theta_{HA})(R_t - B_t) \quad (7)$$

To prevent the model from extracting glimpses from the same location, the model was discouraged from visiting previously attended locations. This is achieved by essentially “blacking out” regions from where the previous glimpses have been extracted within the down sampled image tile i_d which provides contextual information to the model. An additional term was introduced where the sum of the overlapping bounding boxes for the glimpse the locations was calculated. This term was incorporated into the final loss function to encourage the model to select spatially distinct locations.

$$L_{bb} = \frac{1}{T C_2} \sum_{t=0}^T \sum_{tb=t+1}^T b(g_t) \cap b(g_{tb}) \quad (8)$$

where $T C_2$ is the number of possible combinations of T distinct objects taken 2 at a time and b denotes a function that calculates the bounding box around glimpse g at time-step t .

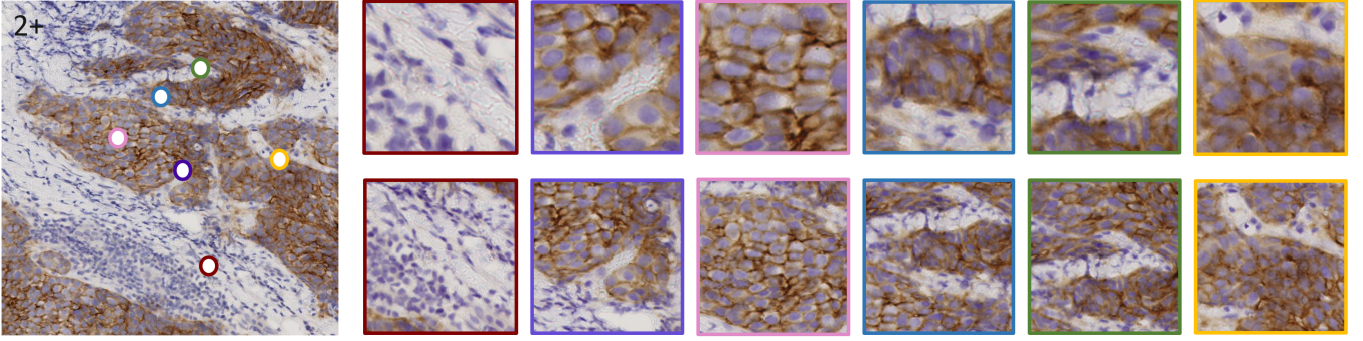


Fig. 4. The first image is an example of an image tile with the locations of six glimpes or patches shown with colored circles for the prediction of HER2 score 2+. The remaining images show the glimpes extracted at the circled locations at resolution 40 \times and 20 \times .

Moreover, to penalize wrong predictions in accordance with their clinical significance, an additional task-specific regularization term was added, $L_s = |Y_t - GT|$.

L_s is a measure of the absolute difference between the ground truth values and the predicted values, considering both are numerical scores. Therefore, this particular component in the loss function will penalize the model based on how "far apart" the ground truth and predicted values are.

Finally, these losses are trained as in (9), where δ is used to control the effect of L_s and L_{bb} .

$$L_{HA} = L_\theta + \delta(L_{bb} + L_s) \quad (9)$$

F. Joint Loss Function

We have trained our model with both components being trained separately and together to demonstrate the flexibility of our proposed framework.

In the absence of an explicit stopping criteria, we have proposed a method of training both components simultaneously. Since the retina-inspired classification model takes much longer to train than the soft attention model, the loss of the soft attention model is incorporated into the final loss function using a decaying coefficient. This allows us to train the model end-to-end with a dynamic loss function [27].

The joint loss function is as in (10), where, $\alpha \in R$ denotes a hyperparameter and e denotes the epoch number.

$$L_J = L_{HA} + (\alpha^e \times L_{SA}) \quad (10)$$

IV. EXPERIMENTAL RESULTS

We have employed our proposed model on two separate use-cases, HER2 prediction for invasive breast carcinoma and the prediction of the Loss/Intact Status of two MMR biomarkers, MLH1 and PMS2.

A. Prediction of HER2 Expression Status in Breast cancer

1) *Dataset*: The experiments were carried out on the HER2 Scoring Contest dataset [28]. The HER2 challenge dataset is publicly available, covered by the Nottingham Research Ethics Committee 2 approval no. REC 2020313 (R&D reference 03HI01). The contest dataset comprised of a total number of 172 WSIs obtained from 86 invasive breast cancer cases.

Each case contains an IHC stained HER2 slide and the corresponding H&E slide. Similar to routine clinical practice, for our experiments, we only take the IHC-stained slides into consideration for assigning HER2 scores. The training dataset consisted of 52 cases, with 13 cases belonging to each of the four scores, while 28 cases were reserved as part of the test data-set. On average the images were made up of approximately 10^{10} pixels and were scanned using the Hamamatsu NanoZoomer C9600. The WSIs possessed a multi-resolution pyramidal structure in the range 4 \times to 40 \times . The GT for each case was obtained from clinical reports marked by at-least two histopathologists and included the slide-level HER2 score for each case (0 – 3+). For our experiments, we performed four-folds cross-validation with the training dataset to create our training and validation data and have used the 28 slides in the contest testing dataset as the test data [28].

2) *Pre-processing and Experimental Setup*: The WSIs were down-sampled by a factor of 32 to level 5 at resolution 2.5 \times as I_0 . In order to prevent the attention model from focusing on any tissue artifacts present in the slide, a tissue mask was generated and applied to each image I_0 using Otsu thresholding and morphological operations [29].

The soft attention model comprises of four convolutional layers followed by rectified linear (ReLU) activation functions, channels were progressively doubled in each subsequent layer. To reduce the size of the sampling space max-pooling was applied to the output of the convolutional layers. Both the initial size of the channels and the size of max pooling kernel was set as 8. A residual network with 8 layers and 32 channels was used for the extraction of features [16].

The parameters high and low for the noise vector were set to range $[0, 1]$. Since we aim to find the "most attentive" regions in a given WSI, the addition of negative noise could be considered counterproductive. The minimum area threshold was set to 20 tiles, where initially we select 20 locations and then we distill 10 spatially distinct tiles by identifying the tiles with the maximum euclidean distance.

To ensure a fair comparison, we have tried to keep the values of the hyperparameters of the classification model similar to the original configuration [12]. Each of the 10 coordinate pairs L_F was mapped to a location in the original WSI using a scale factor $s = 32$. The image tiles i of size 2048 \times 2048 \times 3 were extracted at resolution 40 \times . Furthermore,

TABLE I. HER2 Comparative Results

Teams	Points	W.C.	C.Pts
The proposed method	402.5	23.59	347.2
Learning Where to See [12]	405	24.1	359.1
VISILAB-I (GoogleNet [31])	382.5	23.55	348
FSUJena [23]	370	23	345
HUANGCH (AdaBoost)	377.5	22.62	345.7
MTB NLP (AlexNet[32])	390	22.94	335.7
VISILAB-II (contour analysis)	377.5	21.88	322
Team Indus (LeNet[33])	402.5	18.45	321.4
UC-CCSE [34]	390	21.07	316
MUCS-III [25]	390	20.43	300.8
MUCS-II (GoogleNet [31])	385	19.51	290.1

we performed standard data augmentations : random rotations (0, 90, 180, 270) and horizontal and vertical flipping on the extracted image tiles. During training, in each mini-batch step 40 image tiles were extracted from four down sampled images of different HER2 scores [0 – 3+], resulting in an equal representation of all scores in a single batch. Given a single image tile i from the batch, we extract six sequential multi-resolution glimpses of size $128 \times 128 \times 3$ at magnification levels $20 \times$ and $40 \times$. The location of the first glimpse was selected randomly. The combined representation of the glimpse’s image and location features were of size 1×256 and the hidden layers of the RNN contained 256 and 128 neurons.

The Adam (Kingma & Ba) optimizer [30] and the StepLR scheduler was used for training the model. The learning rate for the soft attention module was initially set to 0.0001 and the hard attention module was set to 0.001. In our experiments we set the value of the regularizer as 1 and in the joint loss experiments, we set the value of alpha as 0.5.

3) *Results*: As in the HER2 scoring contest [28], we have evaluated the performance of the proposed method using three separate criteria, namely a) agreement points, b) weighted confidence and c) combined points. For the first assessment criterion of agreement points, a total of 15 points were awarded based on the variation between the ground truth HER2 labels and the predicted HER2 scores for each case. The second assessment criterion of weighted confidence was used to evaluate the reliability of the predictions by weighing each predicted score with a corresponding confidence value. The third criterion, combined points was calculated by taking a product of the two preceding criteria for each case.

We have used agreement points as the main metric for the evaluation of the proposed model. For the 10 tiles extracted per WSI, the most dominant class was selected as the slide-level score. Mean aggregation was used to aggregate the results of the four folds to arrive at a final HER2 slide-level score for each WSI in the testing dataset. The confidence value was obtained by calculating the average probability values of the 10 tiles extracted for each WSI for each fold.

The proposed model, as shown in Table I achieved a total number of 402.5 points. Our method outperformed other proposed approaches with a significant margin and achieved

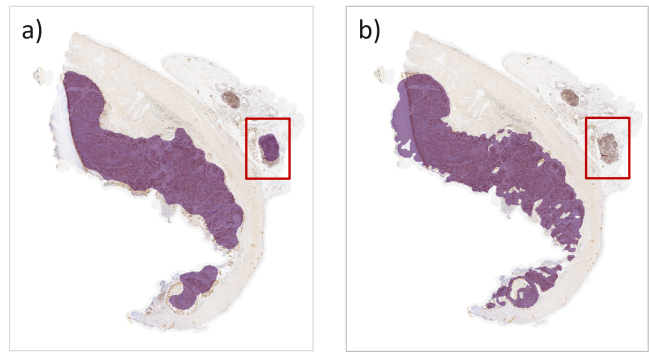


Fig. 5. a) The predicted tumor mask overlay on the WSI with the red box indicating the visual artifacts incorrectly included in the mask; b) The ground truth tumor mask.

comparable performance to [12]. It is important to highlight that [12] extracted approximately 58,000 image tiles whereas our model achieved similar results while only extracting 510 image tiles ($< 1\%$ of image tiles) with the help of attention mechanisms.

B. Prediction of MMR Marker Status in Colon Cancer

1) *Dataset*: This set of experiments was performed on an internal dataset, COMET-MMR dataset, which comprises of 72 WSIs obtained from patients with colorectal cancer. The COMET dataset was collected using the East Midlands Research Ethics Committee (reference 11/WM/0170). The slides were scanned using the Omnyx VL120 scanner and stained with 4 MMR markers. For this IHC study, we only considered the MLH1 and PMS2. The dataset consisted of 14 negative (loss) cases and 58 positive (intact) cases for both MLH1 and PMS2. For our experiments, we performed five-folds cross-validation to create our training, validation and testing datasets. The GT for the WSI level MMR scores were provided by an expert pathologist[35].

2) *Pre-processing and Experimental Setup*: The same experimental setup mentioned previously in Section IV-A2 has been used for these experiments with slight modifications.

The soft attention network consisted of a five-layer CNN, starting with 8 channels. Channels were doubled in each subsequent layer and like before ReLu activation functions were used. A max-pooling layer of size 3 was used to reduce the size and a softmax layer was used to assign probability values. The same networks mentioned previously were used for feature extraction.

Unlike the HER2 Challenge dataset, the IHC stained slides present in the COMET-MMR dataset contained many visual artifacts, some of which escaped the preceding tissue masking steps, e.g. blood vessels and tissue folds. The soft attention model with multinomial entropy was susceptible to focusing on these diagnostically irrelevant structures. While these can be removed using manual masks, in order to show the robustness of the proposed model, it was trained with these artifacts both during training and test time. An example of such artifacts and the corresponding attention masks and GT tumor masks are shown in Fig. 5. However, to reduce the probability of

these structured being picked up by the attention sampling model, negative noise was introduced into our workflow: the parameters *high* and *low* for the noise vector were set as -2 to 1 . Once we obtained the attention maps, k -means clustering with number of clusters = 3 was used to separate the distinct regions namely high attention areas, low attention areas and background region. From the high attention areas 30 locations were pooled to shortlist 15 spatially distinct tiles as L_f . Unlike HER2 where there was no explicit stopping criterion for the attention model, in this dataset we used the dice score loss of the predicted tumor mask with the GT masks to decide when to stop the training of the attention model.

3) Baseline Experiments:

a) *Random Sampling Method*: To evaluate the performance of our dual attention model we have proposed a baseline experiment by randomly extracting image tiles of size 2048×2048 at resolution 40x, without replacement, from the tissue area of the image. The tiles were extracted without using soft attention by using the Gumbel-max trick [36]. The image tiles were then passed to the RL-based hard attention component explained in Section III-D to obtain a classification prediction. The input images and the experimental setup of the RL-based hard attention classifier are the same as in the proposed model.

b) *Sliding Window Method (weakly supervised learning)*: To further compare the performance of our proposed framework, we proposed a second DAB mask based ResNet18 [37] baseline experiment. For each WSI, after the application of a tissue mask, a DAB mask was created by using a threshold of 0.85 on a grayscale image. After the application of both masks, patches of size 224×224 with a tissue area threshold of greater than 0.35 were extracted using the sliding window approach with no overlap. The patches were extracted at magnification $20\times$ in order to incorporate more contextual information.

4) *Results*: We choose F1-score as the main metric for the evaluation of our proposed method. For both the dual attention model and the Random Sampling baseline method we calculated the average probabilities of the 15 tiles selected per WSI to calculate the F1-scores and AUROC scores. For the Sliding Window baseline, for each slide, the top 15 probability values were used. Five-folds cross validation was performed with the same folds used in all the experiments, to ensure a fair comparison.

The comparison of our proposed model with the baseline experiments is shown in Table II where our model outperforms the other techniques with an F1-scores of 0.883 and 0.817 for the biomarkers MLH1 and PMS2, respectively. The second best performing network is Sliding Window method and the lowest performance was achieved by the Random Sampling method. The superior performance of our model can be attributed to the fact that we selectively process only those image tiles that are identified by the soft attention module as potential ROI. Whereas, the poor performance of the Random Sampling Method is due to the fact that the randomly sampled image tiles may include noise from non-tumor areas. This exhibits the advantage of using soft attention during the sampling process, when the same input was provided to both frameworks.

TABLE II. MMR Status Prediction : Comparison with Baselines

Biomarker	Method	F1-Score	AUROC
MLH1	Proposed Method	0.88 ± 0.09	0.92 ± 0.09
	Random Sampling	0.66 ± 0.06	0.67 ± 0.12
	Sliding Window	0.72 ± 0.07	0.92 ± 0.04
PMS2	Proposed Method	0.82 ± 0.08	0.89 ± 0.09
	Random Sampling	0.62 ± 0.11	0.64 ± 0.04
	Sliding Window	0.71 ± 0.09	0.93 ± 0.08

Regarding the AUROC scores, it can be seen from Table II that the proposed model achieves equivalent performance to the Sliding Window baseline model. The performance of the proposed model is comparable for the biomarker MLH1 whereas in PMS2 it lags behind by a margin of approximately 1%. The AUROC and F1-scores for this model can be explained by the fact that it ranks the test samples in the unbalanced dataset better at higher thresholds. The application of DAB masks as a pre-processing step for the Sliding Window baseline also brings about a significant advantage for the scoring of IHC stained slides by reducing the amount of noise, as compared to the random-sampling procedure. It is important to note here that the Sliding Window baseline extracts patches from the entire image whereas our model uses only 15 tiles for a single image.

The first of the two baselines, random sampling aims to showcase the efficacy of the soft attention component of our proposed model and to exhibit the advantage of employing an attention mechanism in comparison to randomly extracting tiles. The second baseline, Sliding Window, follows the standard CPATH pipeline. The motivation behind the selection of this baseline was to demonstrate that we can achieve performance comparable to that of the standard CPATH methods without needing to process the entire WSI, which is both computationally inefficient and time-consuming.

V. CONCLUSIONS

In this study, we have presented a novel dual attention model that combines soft attention at the slide level and hard attention at the patch level for automated scoring of IHC stained WSIs. We model a pathologist’s visual analysis of a WSI, by first employing a soft attention mechanism at low resolution to identify areas in need of further investigation and then extracting a set of spatially distinct and diverse image tiles from these regions. Additionally, instead of processing these extracted tiles entirely, we further employ reinforcement learning to extract a sequence of saccades to score each tile. These scores are then aggregated to reach a slide-level classification decision. We trained the two attention modules both separately and together for two IHC datasets, where the binary prediction of the Loss/Intact status for the MLH1 and PMS2 biomarkers in colorectal cancer is dependent on the presence of DAB staining and HER2 scoring in breast cancer is associated with the intensity of DAB staining. Conventional WSI pre-processing pipelines employ the sliding window paradigm, where the standard approach is to independently extract and save the image patches. Not only is this a time-consuming task but it requires vast reserves of memory. We

take inspiration from the principle of “working smarter, not harder”, and achieve results comparable to the state-of-the-art methods while only processing a fraction of the WSI at the highest resolution. While the average WSI can be of the order of 10^{10} pixels, we perform slide-level classification while only attending to less than 20 glimpses of size 128×128 each, at the highest resolution ($40\times$ and $20\times$) from a single slide, which amounts to less than 5% of the entire slide area, while achieving results comparable to conventional methods.

The proposed method also attempts to address the memory issues inherent in all patch-based models, by extracting a batch of image tiles in real time, performing the required analysis, updating the gradients accordingly and then discarding the image tiles without saving them, potentially saving memory. This can allow for the deployment of this method in labs with limited memory resources. Additionally, in standard WSI pipelines which extract hundreds of image tiles per slide, it is difficult to ascertain which tiles have contributed to the final score. In comparison, our selective attention mechanism which identifies truly useful image tiles, can allow a pathologist to conveniently assess and corroborate the predicted results and can be incorporated as an assistive diagnostic tool. An open problem is how to select the optimal number of tiles extracted from each slide for slide-level classification.

REFERENCES

- [1] P. Brandtzaeg, “The increasing power of immunohistochemistry and immunocytochemistry,” *Journal of immunological methods*, vol. 216, no. 1-2, pp. 49–67, 1998.
- [2] A. E. Rizzardi, A. T. Johnson, R. I. Vogel, S. E. Pambuccian, J. Henriksen, A. P. Skubitz, G. J. Metzger, and S. C. Schmechel, “Quantitative comparison of immunohistochemical staining measured by digital image analysis versus pathologist visual scoring,” *Diagnostic pathology*, vol. 7, no. 1, pp. 1–10, 2012.
- [3] N. L. Henry and D. F. Hayes, “Cancer biomarkers,” *Molecular oncology*, vol. 6, no. 2, pp. 140–146, 2012.
- [4] R. Neve, H. Lane, and N. Hynes, “The role of overexpressed her2 in transformation,” *Annals of oncology*, vol. 12, pp. S9–S13, 2001.
- [5] C. A. Hudis, “Trastuzumab—mechanism of action and use in clinical practice,” *New England journal of medicine*, vol. 357, no. 1, pp. 39–51, 2007.
- [6] D. L. Worthley and B. A. Leggett, “Colorectal cancer: molecular features and clinical opportunities,” *The Clinical Biochemist Reviews*, vol. 31, no. 2, p. 31, 2010.
- [7] L. L. De Matos, D. C. Truffelli, M. G. L. De Matos, and M. A. da Silva Pinhal, “Immunohistochemistry as an important tool in biomarkers detection and clinical practice,” *Biomarker insights*, vol. 5, pp. BMI–S2185, 2010.
- [8] M. K. K. Niazi, A. V. Parwani, and M. N. Gurcan, “Digital pathology and artificial intelligence,” *The lancet oncology*, vol. 20, no. 5, pp. e253–e261, 2019.
- [9] L. King, “How does a pathologist make a diagnosis?” *Archives of Pathology*, vol. 84, no. 4, pp. 331–333, 1967.
- [10] G. P. Pena and J. S. Andrade-Filho, “How does a pathologist make a diagnosis?” *Archives of pathology & laboratory medicine*, vol. 133, no. 1, pp. 124–132, 2009.
- [11] R. S. Bashir, H. Mahmood, M. Shaban, S. E. A. Raza, M. M. Fraz, S. A. Khurram, and N. M. Rajpoot, “Automated grade classification of oral epithelial dysplasia using morphometric analysis of histology images,” in *Medical Imaging 2020: Digital Pathology*, vol. 11320. SPIE, 2020, pp. 245–250.
- [12] T. Qaiser and N. M. Rajpoot, “Learning where to see: A novel attention model for automated immunohistochemical scoring,” *IEEE transactions on medical imaging*, vol. 38, no. 11, pp. 2620–2631, 2019.
- [13] H. Yang, J.-Y. Kim, H. Kim, and S. P. Adhikari, “Guided soft attention network for classification of breast cancer histopathology images,” *IEEE transactions on medical imaging*, vol. 39, no. 5, pp. 1306–1315, 2019.
- [14] B. Xu, J. Liu, X. Hou, B. Liu, J. Garibaldi, I. O. Ellis, A. Green, L. Shen, and G. Qiu, “Attention by selection: A deep selective attention approach to breast cancer classification,” *IEEE transactions on medical imaging*, vol. 39, no. 6, pp. 1930–1941, 2019.
- [15] F. Kong and R. Henaou, “Efficient classification of very large images with tiny objects,” in *Proceedings of the IEEE/CVF Conference on Computer Vision and Pattern Recognition*, 2022, pp. 2384–2394.
- [16] A. Katharopoulos and F. Fleuret, “Processing megapixel images with deep attention-sampling models,” in *International Conference on Machine Learning*. PMLR, 2019, pp. 3282–3291.
- [17] J. Zhang, K. Ma, J. Van Arnam, R. Gupta, J. Saltz, M. Vakalopoulou, and D. Samaras, “A joint spatial and magnification based attention framework for large scale histopathology classification,” in *Proceedings of the IEEE/CVF Conference on Computer Vision and Pattern Recognition*, 2021, pp. 3776–3784.
- [18] V. Mnih, N. Heess, A. Graves *et al.*, “Recurrent models of visual attention,” *Advances in neural information processing systems*, vol. 27, 2014.
- [19] J. Ba, V. Mnih, and K. Kavukcuoglu, “Multiple object recognition with visual attention,” *arXiv preprint arXiv:1412.7755*, 2014.
- [20] A. BenTaieb and G. Hamarneh, “Predicting cancer with a recurrent visual attention model for histopathology images,” in *International Conference on Medical Image Computing and Computer-Assisted Intervention*. Springer, 2018, pp. 129–137.
- [21] B. Xu, J. Liu, X. Hou, B. Liu, J. Garibaldi, I. O. Ellis, A. Green, L. Shen, and G. Qiu, “Look, investigate, and classify: a deep hybrid attention method for breast cancer classification,” in *2019 IEEE 16th international symposium on biomedical imaging (ISBI 2019)*. IEEE, 2019, pp. 914–918.
- [22] R. Mukundan, “Analysis of image feature characteristics for automated scoring of her2 in histology slides,” *Journal of Imaging*, vol. 5, no. 3, p. 35, 2019.
- [23] E. Rodner, M. Simon, and J. Denzler, “Deep bilinear features for her2 scoring in digital pathology,” *Current Directions in Biomedical Engineering*, vol. 3, no. 2, pp. 811–814, 2017.
- [24] M. Saha and C. Chakraborty, “Her2net: A deep framework for semantic segmentation and classification of cell membranes and nuclei in breast cancer evaluation,” *IEEE Transactions on Image Processing*, vol. 27, no. 5, pp. 2189–2200, 2018.
- [25] T. Pitkääho, T. M. Lehtimäki, J. McDonald, T. J. Naughton *et al.*, “Classifying her2 breast cancer cell samples using deep learning,” in *Proc. Irish Mach. Vis. Image Process. Conf.*, 2016, pp. 1–104.
- [26] D. Eriksson and F. Hu, “Whole-slide image preprocessing in python,” Nov 2018. [Online]. Available: <https://developer.ibm.com/articles/an-automatic-method-to-identify-tissues-from-big-whole-slide-images-pt4/>
- [27] A. Sadafi, A. Makhro, A. Bogdanova, N. Navab, T. Peng, S. Albarqouni, and C. Marr, “Attention based multiple instance learning for classification of blood cell disorders,” in *International Conference on Medical Image Computing and Computer-Assisted Intervention*. Springer, 2020, pp. 246–256.
- [28] T. Qaiser, A. Mukherjee, C. Reddy Pb, S. D. Munugoti, V. Tallam, T. Pitkääho, T. Lehtimäki, T. Naughton, M. Berseth, A. Pedraza *et al.*, “Her 2 challenge contest: a detailed assessment of automated her 2 scoring algorithms in whole slide images of breast cancer tissues,” *Histopathology*, vol. 72, no. 2, pp. 227–238, 2018.
- [29] J. Pocock, S. Graham, Q. D. Vu, M. Jahanifar, S. Deshpande, G. Hadji-georgiou, A. Shephard, R. M. S. Bashir, M. Bilal, W. Lu *et al.*, “Tia-toolbox as an end-to-end library for advanced tissue image analytics,” *Communications medicine*, vol. 2, no. 1, pp. 1–14, 2022.
- [30] D. P. Kingma and J. Ba, “Adam: A method for stochastic optimization,” *arXiv preprint arXiv:1412.6980*, 2014.
- [31] C. Szegedy, W. Liu, Y. Jia, P. Sermanet, S. Reed, D. Anguelov, D. Erhan, V. Vanhoucke, and A. Rabinovich, “Going deeper with convolutions,” in *Proceedings of the IEEE conference on computer vision and pattern recognition*, 2015, pp. 1–9.
- [32] A. Krizhevsky, I. Sutskever, and G. E. Hinton, “Imagenet classification with deep convolutional neural networks,” *Advances in neural information processing systems*, vol. 25, 2012.
- [33] Y. LeCun *et al.*, “Lenet-5, convolutional neural networks,” URL: <http://yann.lecun.com/exdb/lenet>, vol. 20, no. 5, p. 14, 2015.
- [34] R. Mukundan, “Image features based on characteristic curves and local binary patterns for automated her2 scoring,” *Journal of Imaging*, vol. 4, no. 2, p. 35, 2018.
- [35] R. Awan, M. Nimir, S. E. A. Raza, J. Lotz, D. Snead, A. Robison, and N. M. Rajpoot, “Deep learning based prediction of msi in colorectal cancer via prediction of the status of mmr markers,” *arXiv preprint arXiv:2203.00449*, 2022.

- [36] R. Adams, “The gumbel-max trick for discrete distributions,” 2013.
- [37] K. He, X. Zhang, S. Ren, and J. Sun, “Deep residual learning for image recognition,” in *Proceedings of the IEEE conference on computer vision and pattern recognition*, 2016, pp. 770–778.